

Recombination-induced voltage-dependent photocurrent collection loss in CdTe thin film solar cell

Ling-Ling Wu(吴玲玲), Guang-Wei Wang(王光伟), Juan Tian(田涓), Dong-Ming Wang(王东明), and De-Liang Wang(王德亮)

Citation: Chin. Phys. B, 2022, 31 (**10**): 108803. DOI: 10.1088/1674-1056/ac728e
Journal homepage: http://cpb.iphy.ac.cn; http://iopscience.iop.org/cpb

What follows is a list of articles you may be interested in

Development of ZnTe film with high copper doping efficiency for solar cells

Xin-Lu Lin(林新璐), Wen-Xiong Zhao(赵文雄), Qiu-Chen Wu(吴秋晨), Yu-Feng Zhang(张玉峰), Hasitha Mahabaduge, and Xiang-Xin Liu(刘向鑫)
Chin. Phys. B, 2022, 31 (**10**): 108802. DOI: 10.1088/1674-1056/ac6b27

Optical simulation of $CsPbI_3$/TOPCon tandem solar cells with advanced light management

Min Yue(岳敏), Yan Wang(王燕), Hui-Li Liang(梁会力), and Zeng-Xia Mei (梅增霞)
Chin. Phys. B, 2022, 31 (**8**): 088801. DOI: 10.1088/1674-1056/ac693d

A 9% efficiency of flexible Mo-foil-based $Cu_2ZnSn(S, Se)_4$ solar cells by improving CdS buffer layer and heterojunction interface

Quan-Zhen Sun(孙全震), Hong-Jie Jia(贾宏杰), Shu-Ying Cheng(程树英), Hui Deng(邓辉)\ccclink, Qiong Yan(严琼), Bi-Wen Duan(段碧雯), Cai-Xia Zhang(张彩霞), Qiao Zheng(郑巧), Zhi-Yuan Yang(杨志远), Yan-Hong Luo(罗艳红), Qing-Bo Men(孟庆波), and Shu-Juan Huang(黄淑娟)
Chin. Phys. B, 2020, 29 (**12**): 128801. DOI: 10.1088/1674-1056/abb7fe

Influence of CdS films synthesized by different methods on the photovoltaic performance of CdTe/CdS thin film solar cells

Jun Wang(汪俊), Yuquan Wang(王玉全), Cong Liu(刘聪), Meiling Sun(孙美玲), Cao Wang(王操), Guangchao Yin(尹广超), Fuchao Jia(贾福超), Yannan Mu(牟艳男), Xiaolin Liu(刘笑林), Haibin Yang(杨海滨)
Chin. Phys. B, 2020, 29 (**9**): 098802. DOI: 10.1088/1674-1056/abad22

Influence of interface states, conduction band offset, and front contact on the performance of a-SiC: H(n)/c-Si(p) heterojunction solar cells

Zhi Qiao(乔治), Jian-Li Ji(冀建利), Yan-Li Zhang(张彦立), Hu Liu(刘虎), Tong-Kai Li(李同锴)
Chin. Phys. B, 2017, 26 (**6**): 068802. DOI: 10.1088/1674-1056/26/6/068802

Recombination-induced voltage-dependent photocurrent collection loss in CdTe thin film solar cell

Ling-Ling Wu(吴玲玲), Guang-Wei Wang(王光伟), Juan Tian(田涓),
Dong-Ming Wang(王东明), and De-Liang Wang(王德亮)†

Hefei National Laboratory for Physical Sciences at Microscale, University of Science and Technology of China, Hefei 230026, *China*

(Received 23 February 2022; revised manuscript received 18 May 2022; accepted manuscript online 24 May 2022)

Recently, the efficiency of CdTe thin film solar cell has been improved by using new type of window layer $Mg_xZn_{1-x}O$ (MZO). However, it is hard to achieve such a high efficiency as expected. In this report a comparative study is carried out between the MZO/CdTe and CdS/CdTe solar cells to investigate the factors affecting the device performance of MZO/CdTe solar cells. The efficiency loss quantified by voltage-dependent photocurrent collection efficiency ($\eta_C(V')$) is 3.89% for MZO/CdTe and 1.53% for CdS/CdTe solar cells. The higher efficiency loss for the MZO/CdTe solar cell is induced by more severe carrier recombination at the MZO/CdTe p–n junction interface and in CdTe bulk region than that for the CdS/CdTe solar cell. Activation energy (E_a) of the reverse saturation current of the MZO/CdTe and CdS/CdTe solar cells are found to be 1.08 eV and 1.36 eV, respectively. These values indicate that for the CdS/CdTe solar cell the carrier recombination is dominated by bulk Shockley–Read–Hall (SRH) recombination and for the MZO/CdTe solar cell the carrier recombination is dominated by the p–n junction interface recombination. It is found that the tunneling-enhanced interface recombination is also involved in carrier recombination in the MZO/CdTe solar cell. This work demonstrates the poor device performance of the MZO/CdTe solar cell is induced by more severe interface and bulk recombination than that of the CdS/CdTe solar cell.

Keywords: CdTe solar cell, voltage-dependent photocurrent collection efficiency, interface recombination, bulk recombination

PACS: 88.40.jm, 88.40.hj, 73.50.Gr, 88.40.H– **DOI:** 10.1088/1674-1056/ac728e

1. Introduction

CdTe thin film solar cell has proved to be one of the most competitive thin film photovoltaic devices because of its high conversion efficiency, excellent long-term stability and low cost. The record power conversion efficiency (PCE) of the CdTe solar cell and the module have reached 22.1% and 18.6%, respectively.[1,2] The latest increase in PCE is mainly attributed to redevelopment of device window layer structure, which has dramatically improved short-circuit current (J_{sc}) of devices.[3,4] The CdS thin film is usually used as the window layer in CdTe solar cell. However, with a bandgap (E_g) of 2.45 eV, CdS exhibits parasitic absorption of short wavelength light (< 510 nm).[5,6] This can result in a J_{sc} loss of about 5 mA/cm^2.[7] Researchers has tried reducing parasitic absorption by incorporating moderate oxygen into CdS and/or thinning this layer.[6,8] Recently, alternatives to CdS have been investigated, such as $Mg_xZn_{1-x}O$ (MZO) and CdSe.[9–12]

The MZO proved to be a promising material for window layer of CdTe solar cell, because it has a tunable E_g in a range of 3.37 eV–7.6 eV by varying the Mg content.[13] A window layer material with high E_g can improve spectral response and increase J_{sc}. When the MZO film with an appropriate Mg content contacts CdTe film, a slight spike will be formed in the conduction band (CB) at the p–n junction interface. This slight spike can help reduce the interface recombination and improve carrier collection.[14,15] Munshi *et al.* obtained CdTe solar cell with a maximum conversion efficiency of 18.7% by using $Mg_{0.23}Zn_{0.77}O$ as a window layer.[15] However, high-efficiency MZO/CdTe solar cell has not been reproduced by other research groups. One of the causes is the "S-kink" phenomenon, which is attributed to improper conduction band offset (CBO) between the MZO and CdTe interfaces.[16,17] However, even if the "S-kink" is eliminated, MZO/CdTe solar cell still has a low fill factor (FF). Delahoy *et al.* eliminated "S-kink" by using higher CdTe deposition temperature and a thinner MZO layer. The efficiency of the cells increased from 4.2% to 10.5%.[17] However, the FF increased to 47.8% only. Bittau *et al.* also increased the substrate temperature during CdTe deposition. And higher FF was obtained with an average value about 63%.[18] Since the MZO film was sensitive to the oxygen during the solar cell preparation process,[16,19] several researchers have tried removing oxygen in absorber deposition and/or $CdCl_2$ treatment process. Li *et al.* reported a significant increase in FF from 44.8% to 72.9% through an oxygen-free $CdCl_2$ treatment.[16] Similar work has been done by Ablekim *et al.*, but FF was only raised to 55.4%.[19]

In our previous work,[13] the "S-kink" was eliminated by optimizing MZO preparation and heat treatment process. In this work, a comparative study between MZO/CdTe and CdS/CdTe solar cells with similar efficiency is carried out.

†Corresponding author. E-mail: eedewang@ustc.edu.cn

© 2022 Chinese Physical Society and IOP Publishing Ltd

The PCE loss induced by voltage-dependent current collection ($\eta_C(V')$) is quantified. The time-resolved photoluminescence (TRPL) and the temperature-dependent current density-voltage (J–V–T) are measured and SCAPS simulation is performed to investigate the causes for low FF and poor performance of the MZO/CdTe solar cell. And the result shows that more severe carrier recombination in the MZO/CdTe solar cell is responsible for the worse performance than in the CdS/CdTe solar cell.

2. Experiment

As shown in Fig. 1, the CdTe solar cells had a structure of glass/SnO_2:F(FTO)/window layer/p-CdTe/ZnTe:Cu/Au. The intrinsic SnO_2 interlayer in CdS/CdTe solar cell acted as a high resistance layer. And both window layers were deposited on glass/FTO (14 Ω/sq, NSG) substrates via radio frequency (RF) magnesium sputtering. The thicknesses of SnO_2, CdS, and MZO films were 40, 80, and 60 nm, respectively. The MZO films had an Mg:Zn atomic ratio of 0.1:0.9. The SnO_2, CdS and MZO targets of 99.99% purity were used in this work. The deposition atmosphere was a mixture of O_2 and Ar during sputtering. The volume ratio of O_2 was 40% for SnO_2 deposition and a small quantity of O_2 (1%–6%) was introduced during CdS and MZO sputtering. The as-deposited CdS films were then annealed in $CdCl_2$ atmosphere to obtain high-quality crystal. The P-type CdTe absorption layers (∼ 4-μm thick) were deposited by a homemade close-spaced sublimation (CSS) system. The deposition atmosphere was Ar:O_2 mixture for the CdS/CdTe solar cells. And it was pure Ar for the MZO/CdTe solar cells. Subsequently, both stacks were thermally activated in the presence of $CdCl_2$. Before depositing the back contact films , the activated CdTe surface is chemically etched by nitric-phosphoric solution. Then, a 100-nm-thick Cu-doped ZnTe (ZnTe:Cu) buffer layer and an Au electrode were successively evaporated on the etched CdTe surface. Finally, the solar cells were rapidly annealed to activate the ZnTe:Cu. Notably, because MZO film is very sensitive to oxygen,[16,19,20] oxygen was avoided throughout the preparation of MZO/CdTe solar cells except for MZO depositing.

The morphological microstructures of CdTe films were characterized by using a field emission scanning electron microscope (SEM, SU8200, HITACHI). The current density–voltage (J–V) of all solar cells were measured under standard AM1.5 illumination (1 kW·m^{-2}, 25 °C) by using a solar simulator (Oriel Sol 3A, USA). Two light filters were used to obtain monochromatic light centered at 532 nm with a full width at half maximum (FWHM) of 10 nm and infrared light with wavelength higher than 850-nm irradiation. For simplicity, these illumination conditions are named 1 sun, 532-nm monochromatic and infrared illumination hereinafter. And J–V–T characteristics were performed by using a liquid-N_2-cooled cryostat (LT3-OM). The temperature was in a range of 80 K to 320 K. The capacitance–voltage (C–V), capacitance–frequency (C–f), and impedance spectroscopy were characterized by using a Tonghui TH2829C LCR meter under dark condition at room temperature. External quantum efficiencies (EQE) of the devices were measured on an Oriel Intelligent Quantum Efficiency 200TM measurement system established with a tunable light source. The TRPL were measured by using a time-correlated single-photon counting system (Timeharp 260) under excitation provided by a picosecond pulsed sources (Picoquant Solea) at a wavelength of 600 nm with a repetition frequency of 40 MHz. The time resolution of the TRPL experimental measurements is ∼ 0.24 ns.

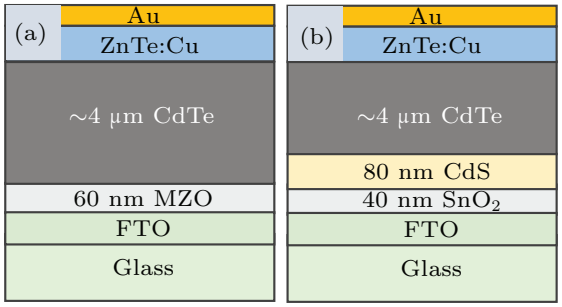


Fig. 1. Schematic representation of CdTe solar cells used in this work: (a) FTO/MZO/CdTe and (b) FTO/SnO_2/CdS/CdTe.

3. Results and discussion

3.1. Solar cell performance

The surface SEM images of CdTe deposited on MZO and CdS are given in Figs. 2(a) and 2(c). The grain sizes (1 μm–2 μm) of polycrystalline CdTe deposited on CdS window layer are more uniform than on MZO, which range from a few hundred nanometers to several micrometers. This can be ascribed to the lack of O_2 in the CdTe deposition process. The O_2 can definitely affect the quality of CdTe film by tuning nucleation, grain size, pinhole formation, and defect chemistry.[19,21–23]

Figures 2(b) and 2(d) show the SEM cross-sectional microstructure of the window layer/CdTe junction region. The MZO layer is composed of densely-packed nanocrystals as shown in Fig. 2(b). The nanocrystals indicate a large number of grain boundaries, which can increase recombination velocity at the p–n junction interface.[14,24] At the CdS/CdTe junction interface, the CdS film consists of mono grains.[25,26] And a thin CdS_xTe_{1-x} layer is formed due to the interdiffusion between CdS and CdTe, which can reduce lattice mismatch and suppress interface recombination. The structural properties are significantly influenced by type and structure of the window layer, such as interface quality, preferential orientation, and grains size of CdTe.[27] And these properties will further affect the photovoltaic performance of cells.

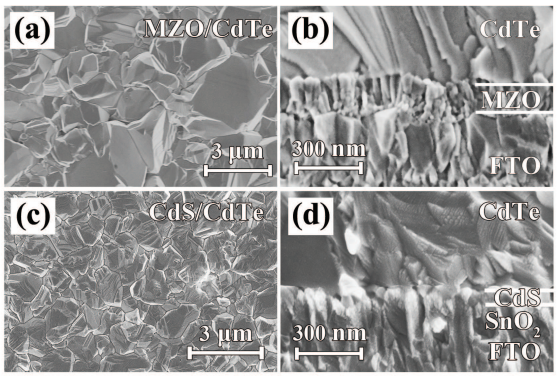


Fig. 2. (a) SEM surface and (b) cross-sectional morphology at the interface of MZO/CdTe solar cell, (c) SEM surface, and (d) cross-sectional morphology at interface of CdS/CdTe solar cells.

The light and dark J–V curves of the MZO/CdTe and CdS/CdTe solar cells with similar efficiencies are shown in Fig. 3(a). Detailed performance parameters are given in Table 1. Notably, neither of the cells shows "roll-over" or "S-kink" phenomenon in their J–V curves. The lack of "S-kink" implies that CBO between the MZO and CdTe is not too high for solar cell devices.[16] The V_{oc} of the MZO/CdTe solar cell is 805 mV, which is 42-mV higher than that of the CdS/CdTe cell. This is consistent with built-in voltage (V_{bi}) result obtained from the x-axis intercept of $1/C^2$–V plots as shown in Fig. 3(b). The J_{sc} of MZO/CdTe solar cell is also a bit lower than that of the CdS/CdTe solar cell, which is counterintuitive as one should reduce optical loss and increase J_{sc} by replacing CdS with MZO.[15]

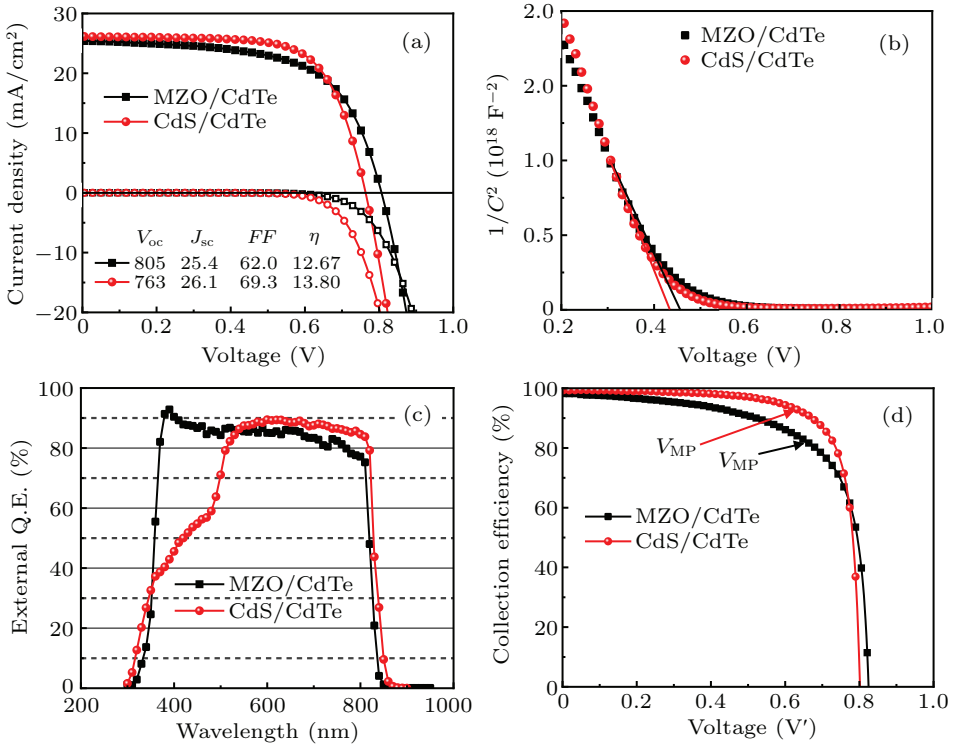


Fig. 3. (a) Light (solid) and dark (hollow) J–V curves, (b) $1/C^2$–V plots, (c) external quantum efficiencies (Q.E.), and (d) collection efficiency of the MZO/CdTe and CdS/CdTe solar cells,with V_{MP} denoting optimum voltage.

Figure 3(c) shows the EQE curves of the two solar cells. The CdS/CdTe solar cell exhibits the typical optical loss in the short wavelength region ($\lambda < 510$ nm) due to parasitic absorption of CdS window layer. As expected, this parasitic absorption is eliminated when CdS is replaced by MZO. However, for the MZO/CdTe devices, EQE loss occurs in the wavelength range of 600 nm–850 nm and this is responsible for failing to achieve high J_{sc} as expected. Generally, the reduced EQE response in this range is called deep-penetration loss, which results mainly from ineffective generation or insufficient carrier collection in bulk region or near back contact. The CdTe films of the devices in this study are all ∼4-μm thick, which is thick enough to absorb 99% photons with energy greater than band gap. Therefore, more significant losses in this range might result from more drastic bulk recombination in the CdTe film of MZO/CdTe solar cell than in CdS/CdTe solar cell. And this can be related to the lack of O_2 in the CdTe film deposition process of MZO/CdTe solar cell.

The current density ($J_{sc,EQE}$) integrated from the EQE data is 23.9 mA/cm^2 for the MZO/CdTe and 23.3 mA/cm^2 for the CdS/CdTe solar cell. The $J_{sc,EQE}$ is lower than the J_{sc} at 1 sun, which results from the different setups for the J–V and spectral response measurements.[28] The $J_{sc,EQE}$ of MZO/CdTe solar cell is higher than that of CdS/CdTe one, which is contrary to their corresponding J–V measurement results. There are two possible reasons for this phenomenon. Firstly, the EQE measurement is carried out in a range of 300 nm–900 nm, but the wavelength of light used in our so-

lar simulator (Oriel Sol 3A) ranges from 400 nm to 1100 nm. The integrated current density calculated by the EQE data in the wavelength range of 300 nm–400 nm of the MZO/CdTe solar cell is ~ 0.3 mA/cm^2 higher than that of CdS/CdTe solar cell. Secondary, both the CdS and CdTe exhibit photoconductivity under 1-sun illumination.[29] But for MZO, the photoconductivity usually occurs when wavelength of the incident light is lower than 400 nm.[30,31] The photoconductivity will increase the donor density in CdS and acceptor density in CdTe. The unchanged donor density in the MZO and increased acceptor density in the CdTe cause the depletion width to decrease. Consequently, the collection of carriers in the MZO/CdTe solar cell generated by the long wavelength light will decrease, while the collection of carriers generated by the long wavelength light will be less affected in the CdS/CdTe solar cell. Therefore, the difference in collection efficiency in the long wavelength range between the MZO/CdTe solar cell and CdS/CdTe solar cell will be lager under 1-sun illumination than under EQE measurement condition.

The PCE of the MZO/CdTe device is 12.67%, a bit lower than that of CdS/CdTe solar cell, 13.80%. The lower PCE is mainly caused by the lower FF. The FF is 62.0% for the MZO/CdTe and 69.3% for CdS/CdTe solar cell. The FF decreases with series resistance ($R_{S,L}$) increasing and with shunt resistance (R_P) decreasing. The $R_{S,L}$ and R_P are calculated from the line slope of the light J–V curves at the open-circuit voltage and short-circuit current points, respectively. As shown in Table 1, under 1-sun illumination the $R_{S,L}$ difference between the two solar cells is only 0.6 Ω·cm^2. But R_P of the CdS/CdTe solar cell is about four times as great as that of the MZO/CdTe. This indicates more severe recombination in the MZO/CdTe solar cell than in the CdS/CdTe solar cell. Besides, the R_p value of the CdTe solar cells is much larger under 532-nm monochromatic light illumination and/or infrared illumination ($\lambda > 850$ nm) than under 1-sun illumination. According to our previous work, this phenomenon might result from the reduced incident light intensity and indicates that the shunting current is induced by the ohmic shunting path rather than the weak diode or space-charge limited current (SCLC).[32]

Table 1. The J–V parameters of CdTe solar cells.

Illumination condition	Window layer	V_{oc} (mV)	J_{sc} (mA/cm^2)	FF (%)	E_{ff} (%)	$R_{S,L}$ (Ω·cm^2)	R_P (Ω·cm^2)
1 sun	MZO	805	25.4	62.0	12.67	4.3	534
	CdS	763	26.1	69.3	13.80	3.7	2103
532-nm monochromatic	MZO	677	1.3	65.4	0.56	54.3	9022
	CdS	629	1.2	71.7	0.52	42.6	23447
Infrared illumination	MZO	643	0.8	59.4	0.30	95.9	5497
	CdS	614	0.9	68.3	0.39	56.3	12521

3.2. Voltage-dependent collection efficiency

3.2.1. Under 1 sun

In order to ascertain the causes for poor performance of the MZO/CdTe solar cell, the voltage-dependent photocurrent collection efficiency, $\eta_C(V')$, is calculated. According to Hegedus,[33] the $\eta_C(V')$ can be calculated from

$$\eta_C(V') = \frac{J_D(V') - J_1(V')}{J_{L01}}, \tag{1}$$

where $J_1(V')$ and $J_D(V')$ are the output currents measured under illumination and in dark condition, respectively; J_{L01} is the ideal photocurrent that can be approximated by J_{sc}, or determined under reverse bias; V is the applied voltage; V' represents the R_S-corrected voltage. The actual voltage across absorption layer should be corrected to $V' = V - R_S \times J(V)$, especially at high forward bias. In this work, R_S is determined from the intercept of dV/dJ *versus* $1/(J + J_{sc})$ by using dark J–V data, and is referred to as $R_{S,D}$.[34]

Generally, collection loss of photocurrent occurs in these regions: space charge region (SCR), neutral region, and interfaces, and it is severely affected by carrier drift, diffusion and recombination.[33,35,36] For the CdTe absorber material, most of light is absorbed in SCR, where the electric field strength is high. Thus, the photo-generated carriers can be effectively separated by electric field when the applied voltage is low. As the applied forward bias increases, both the electric field strength and the width of SCR decrease. Reduction of the electric field strength leads the minority carriers to accumulate, and the carrier recombination to increase by defects at p–n junction interface. Meanwhile, the decrease of SCR width indicates that more light will be absorbed in neutral region. Without electric field, the photo-generated carriers cannot be separated effectively and then the bulk recombination will be enhanced. Figure 3(d) shows $\eta_C(V')$ curves of the foregoing two cells under 1-sun illumination, which are calculated from Eq. (1). The $\eta_C(V')$ for each of the MZO/CdTe and CdS/CdTe solar cells is nearly 100% when the applied voltage is in a range of 0 V–0.2 V. For the applied voltage in a range of 0.2 V–0.7 V, the $\eta_C(V')$ of MZO/CdTe solar cell is lower than that of CdS/CdTe solar cell. The greater collection loss in this region is related to more severe p–n junction interface and/or bulk recombination in MZO/CdTe solar cell. The photocur-

rent collection exhibits the lower loss in the MZO/CdTe solar cell when applied bias increases to around V_{oc}. Because the V_{oc} and V_{bi} in MZO/CdTe are a little higher than in CdS/CdTe solar cell.

Hegedus *et al*. reported that voltage-dependent photocurrent $J_L(V)$ reduces the FF of typical CdS/CdTe solar cell by 10%–15%, V_{oc} by 20 mV–50 mV and efficiency by 2%–4%.[33] The decrement of V_{oc} and FF caused by $J_L(V)$ are calculated according to Eron *et al*.[37] and given below:

$$\Delta V_{oc} = \frac{AkT}{q} \ln \eta_C (V_{oc}), \tag{2}$$

$$\Delta FF = \frac{V_{MP}}{V_{oc}} \left[1 - \eta_C (V_{MP})\right], \tag{3}$$

where $\eta_C(V_{oc})$ and $\eta_C(V_{MP})$ are the collection efficiencies at forward bias of V_{oc} and optimum voltage (V_{MP}) at a maximum power (MP) point, respectively; A, k, T, and q are the ideal factor, Boltzmann constant, temperature, and electron charge, respectively.

The calculated V_{oc} and FF loss caused by $J_L(V)$ of the CdS/CdTe solar cell under 1-sun illumination are 20.2 mV and 5.7%, respectively. And photocurrent loss at MP point is about 7.3% of the J_{sc}. These results give an efficiency reduction of 1.53%. And the efficiency of this cell can increase from 13.80% to 15.33% after correcting for $\eta_C(V')$. The losses in the MZO/CdTe solar cell are much higher, specifically, their values being 51.6 mV, 14.1%, 18.4%, and 3.89% for ΔV_{oc}, ΔFF, photocurrent loss at MP point, and efficiency, respectively. The efficiency of this MZO/CdTe solar cell significantly increases from 12.67% to 16.56% after correcting for $\eta_C(V')$. The more serious efficiency loss might result from the much more severe recombination in the MZO/CdTe solar cell. This is consistent with J–V result that the MZO/CdTe solar cell has a lower shunt resistance.

3.2.2. Under 532-nm monochromatic illumination

Figures 4(a) and 4(b) show the J–V curves measured under 532-nm monochromatic illumination and the corresponding $\eta_C(V')$ curves, respectively. The 532-nm monochromatic light will be absorbed within 100 nm from the layer/absorption layer interface due to high absorption coefficient of CdTe.[38] The carriers excited by 532-nm monochromatic light will be more seriously affected by p–n junction interface recombination. The J–V curves in Fig. 4(a) show that the MZO/CdTe solar cell has higher V_{oc}, J_{sc}, and PCE than CdS/CdTe solar cell. While the $\eta_C(V')$ of the MZO/CdTe cell is lower than that of CdS/CdTe cell when the applied forward bias is in a range of 0 V–0.7 V. This result suggests that there exists more serious p–n junction interface recombination in MZO/CdTe cells than in the CdS/CdTe cells, resulting in lower collection efficiency. The $\eta_C(V')$ of CdS/CdTe cell decreases very slowly when bias voltage is less than V_{oc}. This result indicates that the interface recombination between CdS and CdTe is quite weak. When the voltage is higher than V_{oc}, the electric field strength decreases to zero and the photo-generated carriers will accumulate in SCR and recombine by defects subsequently.

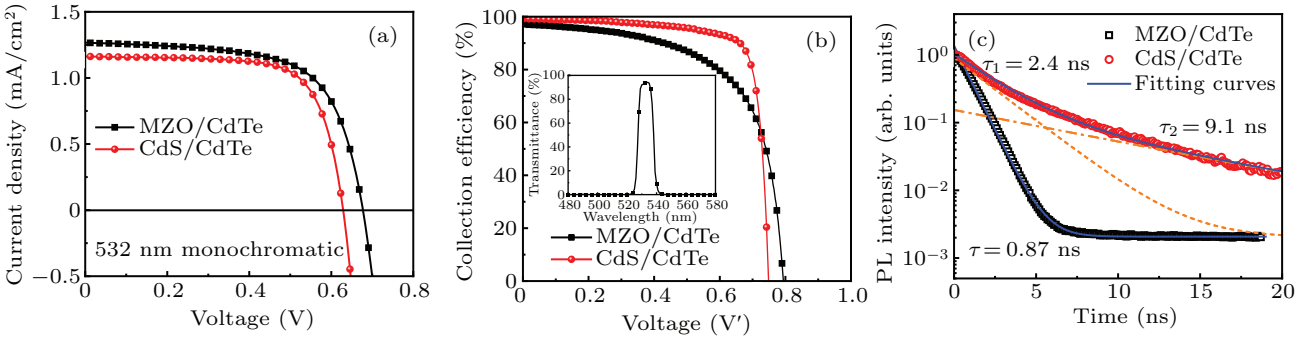


Fig. 4. (a) The J–V curves and (b) collection efficiency of CdTe solar cells under 532-nm monochromatic illumination, with inset showing the transmission spectrum of the 532-nm monochromatic filter. (c) Time-resolved photoluminescence spectra of MZO/CdTe and CdS/CdTe solar cells.

The p–n junction interface recombination significantly affects the carrier lifetime in CdTe. Therefore, the TRPL is measured to compare the interface recombinations of the two solar cells. The incident light with a wavelength of 600 nm is excited from glass side and will be absorbed near the window layer/absorber interface. The TRPL spectra are shown in Fig. 4(c). As can be seen, the CdS/CdTe solar cell exhibits the bi-exponential decay processes with two minority carrier lifetimes of 2.4 ns and 9.1 ns. The initial fast decay τ_1 is attributed to large recombination rate at the p–n junction interface. While the longer decay τ_2 represents the bulk recombination process in the CdTe film.[39] However, the MZO/CdTe solar cell shows only a much shorter carrier lifetime of 0.87 ns. These results prove that the MZO/CdTe solar cell exhibits more serious p–n junction interface recombination.

3.2.3. Under infrared illumination

The SCR width of a typical CdTe cell is in a range of 1 μm–2 μm, while the penetration depth in the CdTe film of light with a wavelength longer than 850 nm is more than 2 μm. Minority carriers excited by this infrared light are generated near the back contact and have to diffuse from neutral region

to SCR before being collected. However, diffusion length is much shorter than drift length in the CdTe.[35] Therefore, carriers excited by infrared light are more likely to be recombined by defects located in CdTe bulk before arriving at p–n junction interface. Figures 5(a) and 5(b) show the J–V curves and $\eta_C(V')$ of the two solar cells under infrared illumination. Although the MZO/CdTe solar cell has higher V_{oc} than the CdS/CdTe solar cell, its $\eta_C(V')$ is much lower in a range of 0 V–0.65 V. The lower $\eta_C(V')$ implies more severe bulk recombination in the MZO/CdTe solar cell than the CdS/CdTe solar cell.

Impedance spectroscopy is a useful tool to investigate carrier recombination at hetero-junction structural interface in solar cell device. In order to study the recombination around CdTe/ZnTe:Cu interface, the impedance spectroscopy is performed. In the measurements, the MZO/CdTe and CdS/CdTe solar cells are biased in the dark under a positive potential of 0.5 V and the applied frequency ranges from 50 Hz to 200 kHz. Figure 5(c) shows the Nyquist plots of the MZO/CdTe and CdS/CdTe solar cells. The inset in Fig. 5(c) shows the equivalent electronic circuit employed to fit the impedance spectra. The equivalent electronic circuit includes a series resistance R_S, a recombination resistance R_{rec}, and a capacitor. As shown in Fig. 5(c), the data can be well fitted with the equivalent electronic circuit. The obtained series resistances for the two solar cells are almost the same. The recombination resistance R_{rec} value is 228 $\Omega\cdot cm^2$ for the MZO/CdTe and 1079 $\Omega\cdot cm^2$ for the CdS/CdTe solar cell. When the applied forward bias is high, the recombination resistance R_{rec} represents the recombination near the back contact . Therefore, the MZO/CdTe solar cell suffers more serious recombination near the back contact interface than the CdS/CdTe solar cell. And the serious recombination near the back contact is responsible for the low EQE values of MZO/CdTe solar cell in the range of 600 nm–850 nm as shown in Fig. 3(c). This is consistent with the photocurrent collection efficiencies of the two solar cells under infrared illumination.

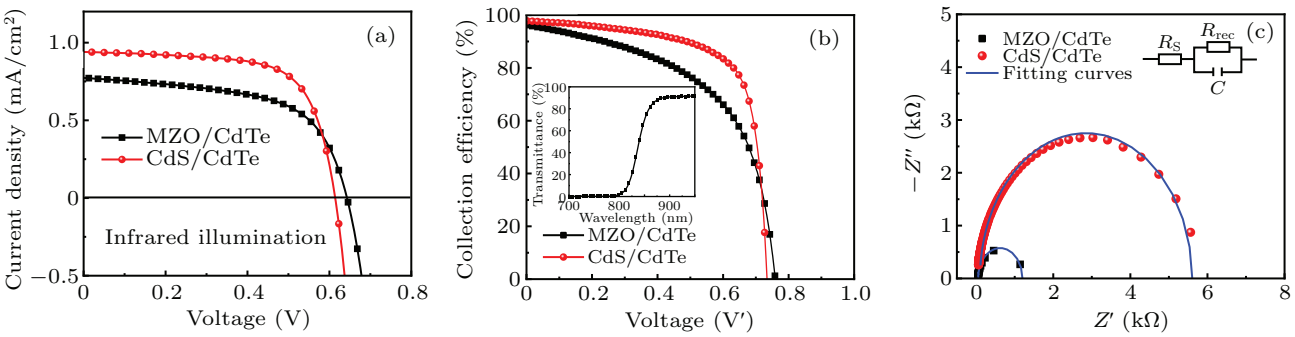


Fig. 5. For MZO/CdTe and CdS/CdTe solar cells, (a) J–V curve, (b) curve of collection efficiency *versus* voltage under infrared illumination, with inset showing the transmission spectra of the infrared filter, and (c) curve of Nyquist plots, with inset showing equivalent electronic circuit model employed to fit the experimental spectrum data.

3.3. Collection loss mechanism

The collection efficiency losses under 532-nm monochromic and infrared illumination indicate more serious recombination both at p–n junction interface and in bulk CdTe near the back contact in the MZO/CdTe solar cell than in the CdS/CdTe solar cell. In order to ascertain which mechanism is dominant in each solar cell, the J–V–T characteristics are carried out. The J–V curves of the MZO/CdTe and CdS/CdTe solar cells, are measured at different temperatures and shown in Fig. 6. None of these curves exhibits "S-kink" phenomenon over the temperature range we tested. The "roll-over" exists at low temperature ($T \leq 250$ K) and results from non-Ohmic back contact. The activation energy E_a of reverse saturation current is obtained by the model that Turcu *et al.* reported.[40] The J_{sc} is a function of V_{oc} expressed as follows:

$$J_{sc} = J_0 \exp\left(\frac{qV_{oc}}{AkT}\right) = J_{00} \exp\left(\frac{qV_{oc}}{AkT}\right) \exp\left(\frac{-E_a}{AkT}\right), \quad (4)$$

where J_0 is the reverse saturation current density, and J_{00} is related to carrier mobility and defect concentration. Thus, V_{oc} can be expressed by,

$$V_{oc} = \frac{E_a}{q} - \frac{AkT}{q} \ln\left(\frac{J_{00}}{J_{sc}}\right). \quad (5)$$

If A, J_{sc}, and J_{00} are temperature-independent, a plot of V_{oc} *versus* T yields a straight line. By extrapolating this line to $T = 0$ K, the activation energy E_a will be obtained. This method has been widely used to determine the activation energy of CdS/CdTe solar cells.[34,41,42] If E_a is smaller than E_g of the absorber material of a solar cell, the recombination is dominant at p–n junction interface. If E_a is similar to E_g of the absorption layer, the recombination is dominant in bulk region.[43] The curves of V_{oc} as a function of temperature (T) for the MZO/CdTe and CdS/CdTe solar cells are plotted in Fig. 7. The E_a values obtained are 1.08 eV and 1.36 eV for the MZO/CdTe and CdS/CdTe solar cells, respectively, indicating that recombination mechanism of the CdS/CdTe solar cell is mainly controlled by Shockley–Read–Hall (SRH) recombination in the bulk region.[43] The E_a value of the MZO/CdTe

solar cell is much lower than 1.45 eV, which implies that the interface recombination is the dominant mechanism in this device.

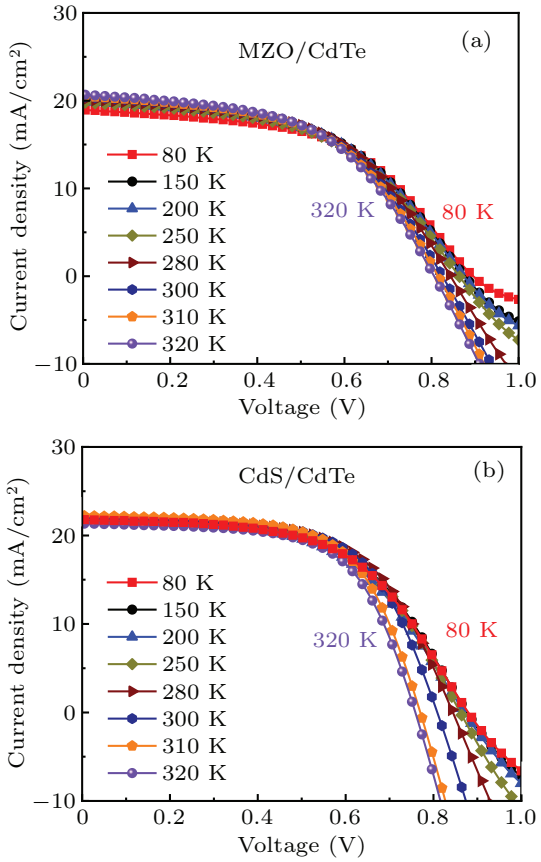


Fig. 6. The *J*–*V* curves of (a) MZO/CdTe solar cells and (b) CdS/CdTe solar cells at different temperatures.

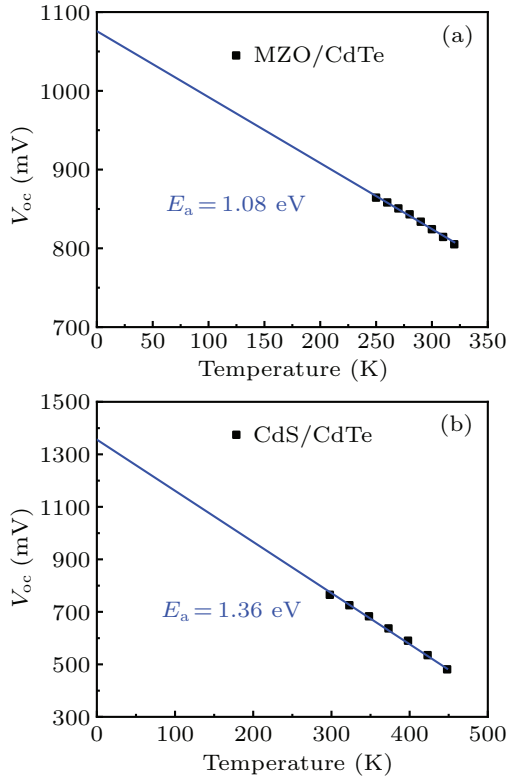


Fig. 7. The V_{oc} as a function of temperature (T) of (a) MZO/CdTe solar cell and (b) CdS/CdTe solar cell.

The tunneling-enhanced interface recombinations widely exist in Cu(In,Ga)Se_2, $CuGaSe_2$, CdTe, and Cu_2ZnSnS_4 thin film solar cells.[44–47] A quantitative analysis was introduced to describe the tunneling at the junction in a Schottky barrier.[48,49] Rau *et al.* extended this model to describe the diode current from pure SRH recombination to tunneling-enhanced interface recombination.[50] In the Padovani–Stratton model, the ideal factor can be described by

$$A = \frac{E_{00}}{kT} \coth\left(\frac{E_{00}}{kT}\right), \tag{6}$$

where E_{00} is characteristic tunneling energy and related to the tunneling probability. The contribution of tunneling increases with E_{00} increasing and T decreasing. When E_{00} is close to kT, the tunneling-enhanced recombination is dominant, while when $E_{00} \ll kT$, pure thermionic emission is dominant.[49,51] In the CdTe solar cell, the thermionic emission refers to the pure SRH recombination.

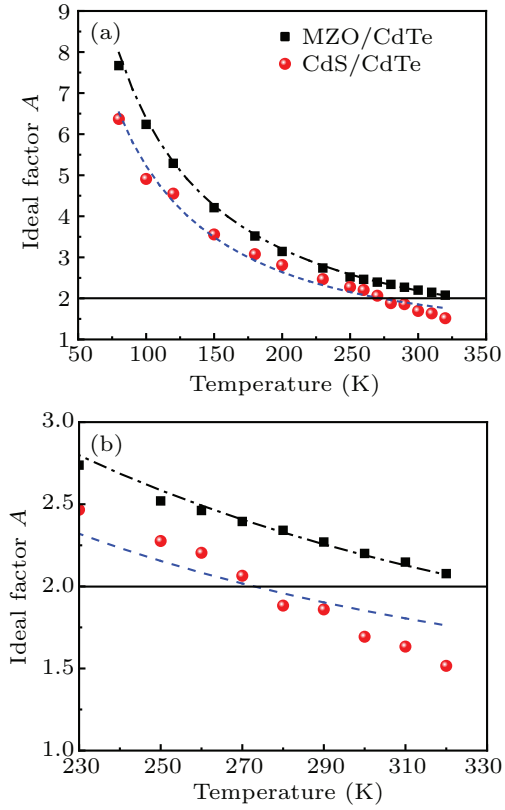


Fig. 8. Plots of ideal factor A *versus* temperature T for MZO/CdTe solar cell and CdS/CdTe solar cell, in a temperature range of (a) 80 K–320 K, and (b) 230 K–320 K.

The ideal factors of the MZO/CdTe and CdS/CdTe solar cells together with fitting curves to Eq. (6) are shown in Fig. 8(a). From these fits the obtained characteristic tunneling energy E_{00} is 55 meV for the MZO/CdTe and 45 meV for CdS/CdTe solar cells. For CdS/CdTe solar cell, equation (6) is not applicable around room temperature as shown in Fig. 8(b). It is believed that tunneling-enhanced interface recombination dominates the reverse saturation current of a

CdS/CdTe solar cell only when the temperature is approximately below 240 K.[45,46] For the MZO/CdTe solar cell, tunneling-enhanced interface recombination is involved over the entire temperature range (80 K$\leq T \leq$320 K) we tested. In our previous work, the electron concentration of MZO film after being annealed is about 10^{18} cm^{-3},[13] which is higher than that in CdS film. Therefore, tunneling is more likely to occur in the MZO/CdTe devices.

3.4. SCAPS simulation

Capacitance–frequency (C–f) response can be used to determine the defect concentration in CdTe absorber.[52,53] Figure 9(a) shows the density of defect states calculated by using a model proposed by Walter *et al.* with C–f data.[54] The peak at the energy of 0.44 eV–0.45 eV is corresponding to the V_{Cd}, or Te_{Cd} or $(Te_{Cd}+2V_{Cd})^{2-}$ defect complex.[55,56] Total defect concentration (N_t) is obtained by integrating the defect distribution curve. The estimated defect concentration of the MZO/CdTe and CdS/CdTe solar cells are 4.53×10^{13} cm^{-3} and 5.15×10^{12} cm^{-3}, respectively. It is reported that the mid-gap defect (about 0.75 eV above the VBM) in the CdTe film plays the main role in degrading cell performance, which is thought to be associated with a complex of V_{Cd}^{2-} and an impurity.[57–59] But it is beyond our C–f testing range. Therefore, SCAPS simulation is carried out to study the influence of interface and bulk SRH recombination on CdTe solar cell performance. Detailed parameters used in simulation are listed in Table 2.[10,13,59,60]

Table 2. Parameters used for SCAPS simulations.

Parameter	MZO	CdS	CdTe
Thickness (nm)	60	50	4000
E_g (eV)	3.53	2.48	1.45
χ (eV)	4.3	4.4	4.4
$\varepsilon/\varepsilon_0$	9	10	9.4
N_C (cm^{-3})	2.2×10^{18}	2.2×10^{18}	8.0×10^{17}
N_V (cm^{-3})	1.8×10^{19}	1.8×10^{19}	1.8×10^{19}
μ_e (cm^2/(V·s))	100	100	320
μ_h (cm^2/(V·s))	25	25	40
n or p (cm^{-3})	n:1.0×10^{18}	n:1.0×10^{17}	p:1×10^{14}

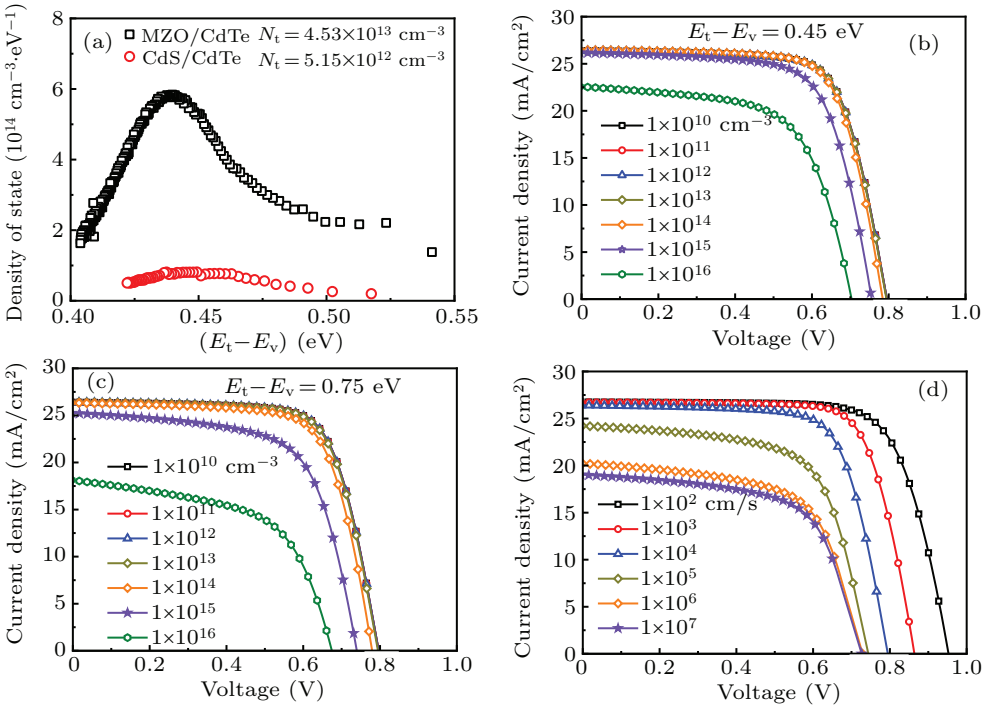


Fig. 9. For MZO/CdTe solar cell and CdS/CdTe solar cell, (a) defect density of state *versus* E_t–E_v, simulation J–V curve for different (b) concentrations of defects at (b) E_{t1}–$E_v = 0.45$, (c) E_{t2}–$E_v = 0.75$ eV, and (d) for interface recombination velocities (S) between CdS and CdTe.

In this one-dimensional simulation, the back contact is assumed to be Ohmic. Figures 9(b)–9(d) show the simulated J–V curves of a CdS/CdTe solar cell with different values of defect concentration (N_t) of a hole trap, E_{t1}, located at 0.45 eV above valence band maximum (VBM), mid-gap defect level, E_{t2}, and interface recombination velocity (S) between the CdS and CdTe, respectively. Both E_{t1} and E_{t2} existed in the bulk CdTe film. As shown in Figs. 9(b) and 9(c), when the concentrations of the two defects are both lower than 10^{14} cm^{-3}, the J–V curves of the cell with different defect concentrations are almost overlapped. When the concentration is higher than 10^{14} cm^{-3}, the performance of the cell will significantly degrade with the increase of defect concentration, especially for the mid-gap defect E_{t2}. According to the C–f measurements, the obtained E_{t1} concentration in the MZO/CdTe solar cell and CdS/CdTe solar cell are both lower than 10^{14} cm^{-3}. Thus, the defect E_{t2} should be responsible for the difference in bulk recombination for CdTe. The device performance shows the

strong correlation with the interface recombination velocity (S) between CdS and CdTe as shown in Fig. 9(d). The V_{oc} of the cell drastically decreases with S increasing. The J_{sc} and FF are influenced by interface recombination only when S is higher than 10^4 cm/s.

Then J–V performance of the MZO/CdTe and CdS/CdTe solar cells shown in Fig. 3(a) are simulated. In the simulation, the concentration of E_{t1} is determined by the C–f measurements. And the influence of concentration of defect E_{t2} and interface recombination velocity are taken into consideration. The simulated curves together with the experimental data are displayed in Fig. 10. From the simulation, the obtained interface recombination velocity of the MZO/CdTe and CdS/CdTe solar cells are 2×10^6 cm/s and 2.4×10^4 cm/s, respectively. This result is consistent with the conclusion derived from TRPL measurements. And the concentration of defect E_{t2} obtained are 2×10^{14} cm^{-3} and 4×10^{13} cm^{-3} for the MZO/CdTe solar cell and CdS/CdTe solar cell, respectively. And this can explain the more severe photocurrent collection loss in MZO/CdTe solar cell under infrared illumination.

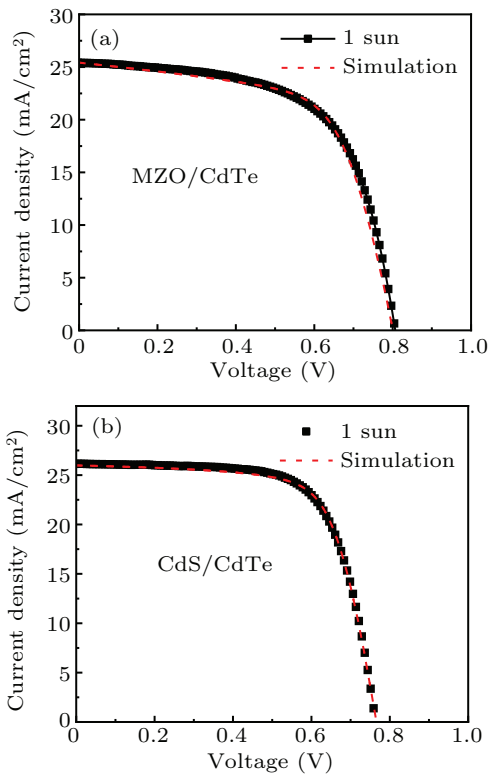


Fig. 10. Experimental J–V data and simulated J–V curves of (a) MZO/CdTe and (b) CdS/CdTe solar cells.

According to the above discussion, the band diagram of MZO/CdTe heterojunction and CdS/CdTe heterojunction under equilibrium state at room temperature are depicted and shown in Figs. 11(a) and 11(b), respectively. We conclude that the bulk SRH recombination in CdTe was dominated in the CdS/CdTe solar cell and the interface recombination is dominated in the MZO/CdTe solar cell. And tunneling enhanced interface recombination is also involved in the MZO/CdTe solar cell at room temperature. The bulk SRH recombination, p–n junction interface recombination, and tunneling-enhanced interface recombination are marked by path 1, path 2, and path 3 in these figures, respectively. And the dominated current mechanism in each solar cell is emphasized by bold arrows.

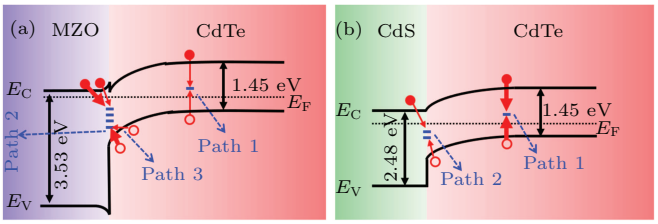


Fig. 11. Band diagram of (a) MZO/CdTe and (b) CdS/CdTe heterojunctions. E_C, E_V, and E_F are the conduction-band-edge, valence-band-edge, and Fermi-level. Paths 1, 2, and 3 are three possible recombination pathways through defects at room temperature, namely, bulk Shockley–Read–Hall recombination, interface recombination, and tunneling-enhanced interface recombination, respectively. The dominant recombination process in each junction is marked by bold arrow.

4. Conclusions

In this work, a comparative study is performed between the MZO/CdTe and CdS/CdTe solar cells with similar performances. It was found that more serious performance loss existed in the MZO/CdTe solar cell than that in the CdS/CdTe solar cell. And this is induced by more severe recombination at the p–n junction interface and in the CdTe bulk region near the back contact. The activation energy is 1.08 eV for the MZO/CdTe solar cell and 1.36 eV for CdS/CdTe solar cell, respectively. This suggests that the bulk SRH recombination in CdTe is dominated in the CdS/CdTe solar cell, while the p–n junction interface recombination is dominated in the MZO/CdTe solar cell. In addition, we also find that the tunneling enhanced interface recombination mechanism is involved in the MZO/CdTe solar cells at room temperature. Moreover, the results of SCAPS simulation support the conclusion that the MZO/CdTe solar cell has a higher interface recombination velocity and bulk defect concentration than the CdS/CdTe solar cell. This work indicates that for poor performance MZO/CdTe solar cell, more efforts should be made to suppress the recombinations both at the p–n junction interface and in bulk CdTe.

Acknowledgement

Project supported by the National Natural Science Foundation of China (Grant Nos. 61774140 and 61474103).

References

[1] Green M A, Emery K, Hishikawa Y, Warta W and Dunlop E D 2016 *Prog. Photovolt.* **24** 3
[2] Green M A, Emery K, Hishikawa Y, Warta W and Dunlop E D 2016 *Prog. Photovolt.* **24** 905

[3] Green M A, Emery K, Hishikawa Y, Warta W and Dunlop E D 2012 *Prog. Photovolt.* **20** 606
[4] Green M A, Emery K, Hishikawa Y, Warta W and Dunlop E D 2015 *Prog. Photovolt.* **23** 1
[5] Wu X 2004 *Sol. Energy* **77** 803
[6] Kephart J M, Geisthardt R M and Sampath W S 2015 *Prog. Photovolt.* **23** 1484
[7] Stephen B, Lukas K, Julian P and Nath T A 2013 *Sol. Energy* **1** 1
[8] Meysing D M, Wolden C A, Griffith M M, Mahabaduge H, Pankow J, Reese M O, Burst J M, Rance W L and Barnes T M 2015 *J. Vac. Sci. Technol. A* **33** 021203
[9] Baines T, Bowen L, Mendis B G and Major J D 2020 *ACS Appl. Mater. Inter.* **12** 38070
[10] Kephart J M, McCamy J W, Ma Z, Ganjoo A, Alamgir F M and Sampath W S 2016 *Sol. Energy Mater. Sol. Cells* **157** 266
[11] Swanson D E, Sites J R and Sampath W S 2017 *Sol. Energy Mater. Sol. Cells* **159** 389
[12] Poplawsky J D, Guo W, Paudel N, Ng A, More K, Leonard D and Yan Y 2016 *Nat. Commun.* **7** 12537
[13] Wang D, Wang G, Cai Y, Wu L, Zhu P and Wang D 2021 *IEEE J. Photovolt.* **11** 974
[14] Ren S, Wang H, Li Y, Li H, He R, Wu L, Li W, Zhang J, Wang W and Feng L 2018 *Sol. Energy Mater. Sol. Cells* **187** 97
[15] Munshi A H, Kephart J M, Abbas A, Shimpi T M, Barth K L, Walls J M and Sampath W S 2018 *Sol. Energy Mater. Sol. Cells* **176** 9
[16] Li D B, Song Z, Awni R A, Bista S S, Shrestha N, Grice C R, Chen L, Liyanage G K, Razooqi M A, Phillips A B, Heben M J, Ellingson R J and Yan Y 2019 *ACS Appl. Energy Mater.* **2** 2896
[17] Delahoy A E, Peng S, Patra P, Manda S, Saraf A, Chen Y, Tan X and Chin K K 2017 *MRS Adv.* **2** 3203
[18] Bittau F, Potamialis C, Togay M, Abbas A, Isherwood P J M, Bowers J W and Walls J M 2018 *Sol. Energy Mater. Sol. Cells* **187** 15
[19] Ablekim T, Perkins C, Zheng X, Reich C, Swanson D, Colegrove E, Duenow J N, Albin D, Nanayakkara S, Reese M O, Shimpi T, Sampath W and Metzger W K 2019 *IEEE J. Photovolt.* **9** 888
[20] Awni R A, Li D B, Song Z, Bista S S, Razooqi M A, Grice C R, Chen L, Liyanage G K, Li C, Phillips A B, Heben M J, Ellingson R J, Li J V and Yan Y 2019 *Prog. Photovolt.* **27** 1115
[21] Korevaar B A, Cournoyer J R, Sulima O, Yakimov A and Johnson J N 2014 *Prog. Photovolt.* **22** 1040
[22] Metzger W K, Albin D, Levi D, Sheldon P, Li X, Keyes B M and Ahrenkiel R K 2003 *J. Appl. Phys.* **94** 3549
[23] Albin D S, Yan Y and Al-Jassim M M 2002 *Prog. Photovolt.* **10** 309
[24] Kaushal A and Kaur D 2009 *Sol. Energy Mater. Sol. Cells* **93** 193
[25] Shen K, Bai Z, Deng Y, Yang R, Wang D, Li Q and Wang D 2016 *RSC Adv.* **6** 52326
[26] Yang R, Wang D, Wan L and Wang D 2014 *RSC Adv.* **4** 22162
[27] Amarasinghe M, Colegrove E, Moseley J, Moutinho H, Albin D, Duenow J, Jensen S, Kephart J, Sampath W, Sivananthan S, Al-Jassim M and Metzger W K 2018 *Adv. Energy Mater.* **8** 1702666
[28] Wienke J, van der Zanden B, Tijssen M and Zeman M 2008 *Sol. Energy Mater. Sol. Cells* **92** 884
[29] Hegedus S, Ryan D, Dobson K, McCandless B and Desai D 2003 *MRS Online Proc. Libr.* **763**
[30] Teherani F H, Look D C, Rogers D J, Schoenfeld W V, Wei M, Boutwell R C and Liu H 2014 *Oxide-based Mater. Devices V* **8987** 329
[31] Yu J, Tian N, Deng Y F and Zhang H H 2016 *J. Alloys Compd.* **667** 359
[32] Shen K, Li Q, Wang D, Yang R, Deng Y, Jeng M J and Wang D 2016 *Sol. Energy Mater. Sol. Cells* **144** 472
[33] Hegedus S, Desai D and Thompson C 2007 *Prog. Photovolt.* **15** 587
[34] Hegedus S S and Shafarman W N 2004 *Prog. Photovolt.* **12** 155
[35] Wang Z, Cheng Z, Delahoy A E and Chin K K 2013 *IEEE J. Photovolt.* **3** 843
[36] Hegedus S S 1997 *Prog. Photovolt.* **5** 151
[37] Hegedus S S 1997 *Prog. Photovolt.* **5** 151
[38] Mitchell K, Fahrenbruch A L and Bube R H 1977 *J. Appl. Phys.* **48** 829
[39] Kuciauskas D, Kanevce A, Burst J M, Duenow J N, Dhere R, Albin D S, Levi D H and Ahrenkiel R K 2013 *IEEE J. Photovolt.* **3** 1319
[40] Turcu M, Pakma O and Rau U 2002 *Appl. Phys. Lett.* **80** 2598
[41] Phillips J E, Birkmire R W, McCandless B E, Meyers P V and Shafarman W N 1996 *Phys. Status Solidi B* **194** 31
[42] Hegedus S S and McCandless B E 2005 *Sol. Energy Mater. Sol. Cells* **88** 75
[43] Chantana J, Kato T, Sugimoto H and Minemoto T 2017 *Prog. Photovolt.* **25** 996
[44] Rau U 1999 *Appl. Phys. Lett.* **74** 111
[45] Bayhan H and Kavasoğlu A S 2005 *Solid-State Electron.* **49** 991
[46] Bayhan H, Dağkaldıran E T, Major J D, Durose K and Bayhan M 2019 *Semicond. Sci. Technol.* **34** 075013
[47] Courel M, Valencia-Resendiz E, Andrade-Arvizu J A, Saucedo E and Vigil-Galán O 2017 *Sol. Energy Mater. Sol. Cells* **159** 151
[48] Padovani F A and Stratton R 1966 *Solid-State Electron.* **9** 695
[49] Jeong S, Song S H, Nagaich K, Campbell S A and Aydil E S 2011 *Thin Solid Films* **519** 6613
[50] Rau U, Jasenek A, Schock H W, Engelhardt F and Meyer T 2000 *Thin Solid Films* **361** 298
[51] Gümüş A, Türüt A and Yalçin N 2002 *J. Appl. Phys.* **91** 245
[52] Proskuryakov Y Y, Durose K, Taele B M and Oelting S 2007 *J. Appl. Phys.* **102** 024504
[53] Fedorenko Y G, Major J D, Pressman A, Phillips L J and Durose K 2015 *J. Appl. Phys.* **118** 165705
[54] Walter T, Herberholz R, Müller C and Schock H W 1996 *J. Appl. Phys.* **80** 4411
[55] Proskuryakov Y Y, Major J D, Durose K, Barrioz V, Irvine S J C, Jones E W and Lamb D 2007 *Appl. Phys. Lett.* **91** 153505
[56] Soundararajan R, Lynn K G, Awadallah S, Szeles C and Wei S H 2006 *J. Electron. Mater.* **35** 1333
[57] Gloeckler M, Fahrenbruch A L and Sites J R 2003 *Proceedings of the 3rd World Conference on Photovoltaic Energy Conversion*, May 11–18, 2003, Osaka, Japan, pp. 491–494
[58] Nardone M and Albin D S 2015 *IEEE J. Photovolt.* **5** 962
[59] Komin V, Tetali B, Viswanathan V, Yu S, Morel D L and Ferekides C S 2003 *Thin Solid Films* **431–432** 143
[60] He X, Song Y, Wu L, Li C, Zhang J and Feng L 2018 *Mater. Res. Express* **5** 065907